JACS
JOURNAL OF THE AMERICAN CHEMICAL SOCIETY
Article
pubs.acs.org/JACS

Nature of Rutile Nuclei in Anatase-to-Rutile Phase Transition

Sheng-Cai Zhu, Song-Hai Xie, and Zhi-Pan Liu*

Collaborative Innovation Center of Chemistry for Energy Material, Shanghai Key Laboratory of Molecular Catalysis and Innovative Materials, Key Laboratory of Computational Physical Science (Ministry of Education), Department of Chemistry, Fudan University, Shanghai 200433, China

Supporting Information

ABSTRACT: The solid phase transition of TiO_2, in particular anatase to rutile, has been extensively studied in the past 30 years. To seek the nucleation site at the beginning of phase transition is highly challenging, which asks for new theoretical techniques with high spatial and temporal resolution. This work reports the first evidence on the atomic structure of the nucleation sites in the TiO_2 anatase-to-rutile phase transition. Novel automated theoretical methods, namely stochastic surface walking based pathway sampling methods, are utilized to resolve the lowest energy pathways at the initial stage of phase transition. We show that among common anatase surfaces, only the (112) ridged surface provides the nucleation site for phase transition, which can lead to the formation of both TiO_2-II and brookite thin slabs. The TiO_2-II phase is kinetically preferred product; the propagation into the subsurface is still hindered by high barriers that is the origin for the slow kinetics of nuclei formation. The rutile nuclei are thus not rutile phase but nascent metastable TiO_2-II phase in an anatase matrix. The phase transition kinetics is found to be sensitive to the compressive strain and the crystallographic directions. The results rationalize the size and morphology dependence of the anisotropic phase transition kinetics of anatase particles and could facilitate the rational design of material via controlled solid phase transition.

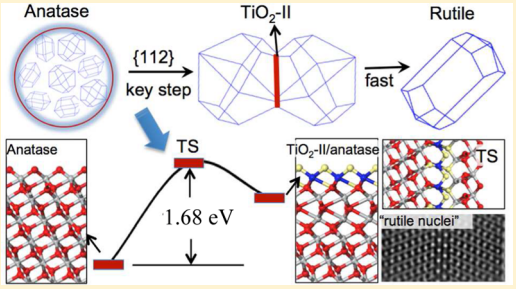

1. INTRODUCTION

Solid surface restructuring occurs ubiquitously in nature, featuring the anisotropic, long-range ordering via collective surface atom movement. The dynamics of surface can lead to the change of nanoparticle morphology and may further initiate the phase transition of solid, which is thus critical for material performance. In titanium oxide (TiO_2), an important material with many applications, e.g., as photocatalysts in water splitting,[1−3] it has been well documented that TiO_2 anatase nanoparticles can undergo solid-to-solid phase transition to form rutile at elevated temperatures. The solid phase transition kinetics is sensitive to a number of factors such as exposed surfaces, nanoparticle size and morphology (see e.g. Figure 1a).[4,5] Because of the complexity of atom displacement patterns in surface restructuring, many fundamental questions on the anatase-to-rutile phase transition kinetics remains elusive. In particular, the structure of rutile nuclei initiating the phase transition is not yet characterized. To understand the anisotropic behavior and predict the crystallographic direction of phase transition kinetics must rank as one of the top concerns in material science.

The phase change of TiO_2 nanoparticle from anatase to rutile (see Figure 1b,c) was widely exploited in synthesizing TiO_2 materials.[6] The phase transition is driven by thermodynamics since anatase ($I4_1/amd$, #141) is more stable as a nanoparticle due to its low surface energies, while rutile ($P4_2/mnm$, #136) is more stable as the bulk phase.[7,8] Although extensively studied, the phase transition kinetics is still much debated (see, e.g., the work by the Banfield group[9−14] and Li group[15,16]), which is apparently due to the complex potential energy surface (PES) of TiO_2. TiO_2 possesses a rich family of possible phases in addition to rutile and anatase, such as brookite (*Pbca*, #61) and TiO_2-II (*Pbcn*, #60).

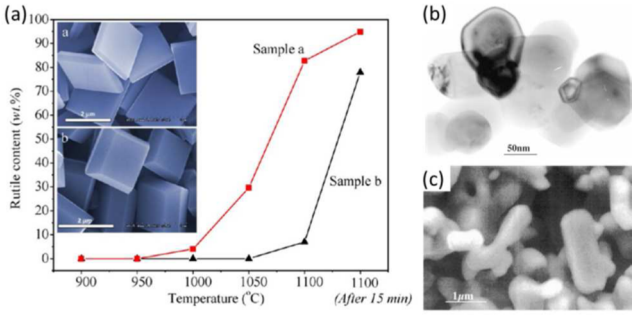

Figure 1. (a) The change of rutile contents with temperature for anatase samples (the insets) with (001) facet percentage of 63% and 32% adapted from ref 4 (Copyright 2014, with permission from American Chemical Society). (b and c) TEM showing the morphology of the anatase powder and the transformed rutile particles adapted from ref 5 (Copyright 2001, with permission from Wiley).

To date, different phase transition mechanisms have been proposed in literature, differing in the pathway of phase transition, e.g., via brookite,[17] TiO_2-II,[18−22] amorphous-phase[23] intermediates, or via a direct pathway without intermediate.[5]

Received: July 23, 2015
Published: August 19, 2015

DOI: 10.1021/jacs.5b07734
J. Am. Chem. Soc. 2015, 137, 11532−11539

Banfield and co-workers,[24,25] using high-resolution TEM (HRTEM), first observed a newly emerged phase that is 3−4 atomic layers thick at the anatase (112) twin interface. This new phase is termed "rutile nucleus" and initiates the phase transformation,[25] which is suggested to be the rate-determining step in the whole phase transition. The relevance of anatase (112) in phase transition was supported recently by force-field molecular dynamics simulation of the anatase nanoparticle,[26] although no intermediate phase was explicitly identified in simulation. In contrast, Xu et al.[27] recently found that the brookite phase can transform to rutile via anatase at 860 °C and ambient pressure and thus suggests a brookite-anatase-rutile indirect pathway. This contradicts apparently with Banfield's suggestion that the transition occurs via the rutile nucleus that is neither anatase nor rutile. On the other hand, other researchers observed TiO_2-II phase attachment on anatase surfaces that can transit to the rutile phase using high-energy impact vibrational ball milling.[18−22] These experiments suggest a new anatase-TiO_2-II-rutile indirect pathway, which was also supported by Dubrovinskaia et al.[28] based on a high-pressure experiment. More recently, Ricci and co-workers[23] found the visible light can also induce the anatase-to-rutile phase transition, and they observed only amorphous intermediates using Raman and photoluminescence technique.

Recently, we investigated the PES of TiO_2 bulk crystals using a novel stochastic surface walking (SSW) for crystal pathway sampling method[29,30] and determined the homogeneous phase transition pathway between different phases (i.e., pathway from A phase to B phase without involving any intermediate A/B heterophase junction).[30,31] We identified the high-pressure phase TiO_2-II as the intermediate in the lowest energy pathway from anatase to rutile, which suggests a crystallographic correspondence between the three phases, i.e. $(101)_R/(001)_{II}$ and $(100)_{II}/(112)_A$[30] (the subscript R, II, A indicate rutile, TiO_2-II, and anatase phases, respectively). Although the homogeneous phase transition pathway confirms the critical role of anatase (112) plane in anatase-to-rutile phase transition, no detailed information can be gleaned for the phase transition kinetics in real scenarios that involve heterogeneous nucleation and anisotropic phase growth.

Considering that the surface restructuring and the subsequent phase transition are the key steps of nucleation, here we extend the SSW method for surface systems and use this state-of-the-art approach to resolve the energy profile of the initial nucleation steps. By exploring systematically surface restructuring of common anatase surfaces, including (001), (100), (101), (112), we show that, while several surfaces can undergo surface reconstruction, only anatase (112) is responsible for the initial nucleation where nascent TiO_2-II and brookite phases with only a few layers thick are formed after surface restructuring. The TiO_2-II is characterized as the rutile nucleus initiating the phase transition. The anisotropic reaction kinetics is observed and rationalized for the first time from energy criterion.

2. THEORETICAL METHODS

2.1. Reaction Pathway Sampling Based on SSW Method. In this work we utilized the SSW pathway sampling method to explore the PES of the surface reconstructing. The pathway sampling combines two methods: the SSW method[32] and the double-ended surface walking (DESW) method.[33] The SSW is for collecting the likely pathways, and the DESW can locate the transition state (TS) of the pathway. This approach was developed recently for predicting the low-energy pathways in molecular reactions and crystal phase transitions. Here we extended the method for surface systems to predict the low-energy pathways of surface reconstruction. The methodology is introduced briefly in the following.

The SSW method[32,34] is an automated approach to explore unbiasedly the multidimensional PES of complex systems by taking into account the second derivative information.[35] The method is originated from the bias-potential driven constrained Broyden dimer (BP-CBD) method for TS searching developed in the group,[34] in which the barrier of reaction is surmounted by adding consecutively Gaussian bias potentials, and the reaction coordinate (the direction where Gaussian is added) is refined continuously using the biased constrained Broyden dimer (biased-CBD) method. In SSW simulation, each SSW step (from one minimum to another) will choose a random direction, and then use the biased-CBD method to refine the direction, along which the structure is perturbed. The SSW parameters utilized in this work are as those utilized previously,[30] namely, the Gaussian width 0.6 Å; maximum 10 Gaussians per SSW steps.

To sample the pathways of surface restructuring, first, we start from one given surface structure (in periodic slab model), e.g., a known unreconstructed crystal surface, defined as the initial state (IS), and utilize the SSW method to explore all the likely surface structure nearby (the lattice is kept fixed during the pathway sampling). The structure selection module is utilized to decide whether to accept/refuse once a new minimum is reached. If a new structure different from the IS structure is identified, we record/output the IS structure together with the final state (FS) structure (e.g., a new phase) of the current SSW step. The difference between two structures is distinguished by multiple criterions, including the symmetry, energy, and Euclidean distance. Then, the program will return back to the IS by rejecting the new minimum to continue the exploration. On the other hand, if the new minimum identified is the same as the starting structure (e.g., the same symmetry but a permutation isomer), the program will accept the new isomeric structure and continue the structure exploration. We repeat the whole procedure until a certain number of IS/FS pairs are collected, typically up to 10^4 pathways being sampled for each surface structure. The purpose of the SSW sampling is to provide a database of the reaction coordinates (IS/FS pairs) describing the pathways of the surface restructuring.

Finally, we utilize the DESW method[34] to identify the TSs explicitly for all the IS/FS pairs.[36] The TS is confirmed by extrapolating the TS toward the IS and FS and the numerical vibrational frequency analysis. The lowest energy pathways are thus determined according to the located TSs by sorting the calculated barrier, the energy difference between the TS and the IS.

2.2. Calculation Details for TiO_2 Systems. Both the classical force-field potential using Matsui−Akaogi (MA) interatomic potential[37] and density functional theory (DFT) calculations have been utilized for the TiO_2 systems. The classical potential calculations are essential for sampling exhaustively the likely phase transition pathways and for obtaining low-energy pathway candidates. The MA potential has been demonstrated to describe reasonably well the phase diagram of TiO_2 at different pressure conditions.[28,37] It should be mentioned that due to the large number of possible reaction pathways for the surface structure reconstruction and the large system size of surface slabs (>90 atoms), the force-field

DOI: 10.1021/jacs.5b07734
J. Am. Chem. Soc. 2015, 137, 11532−11539

simulation is the practical solution for the initial screening of the pathways, where up to 10^4 pathways are sampled for each surface structure. The low-energy pathway candidates obtained using DESW method will be further refined by DFT calculations to obtain accurate energetics of the reaction.

The DFT calculations on the phase transition pathways were performed using the SIESTA package with optimized numerical double-ζ polarization basis set[38,39] at the GGA-PBE exchange–correlation functional level.[40] The energy cutoff for the real space grid used to represent the density was set as 250 Ry. An energy shift of 0.01 eV was used to determine the orbital-confining cutoff radii. For the reconstruction of anatase (112), at least 15 layers of anatase TiO_2 were included to represent the surface with the bottom 9 layers being fixed at the bulk-truncated structure and a vacuum region of more than 10 Å. The **k**-point mesh utilized was up to (4 × 4 × 1) in the Monkhorst–Pack scheme,[41] which was verified to be accurate enough for these surface systems.

3. RESULTS

3.1. Reconstruction of Anatase Surfaces. As the starting point, we utilized the SSW method to explore the likely structures of anatase surfaces, including {101}, {001}, {100}, and {112} (see Figure 2a,b), which are commonly available on anatase decahedron particles synthesized in the experiment. The {101}, {001}, and {100} surfaces are terraces with low surface energies; {112} surface, being 41.2° from {101}, is the ridge separating two neighboring {101} facets, (see Figure 2a).

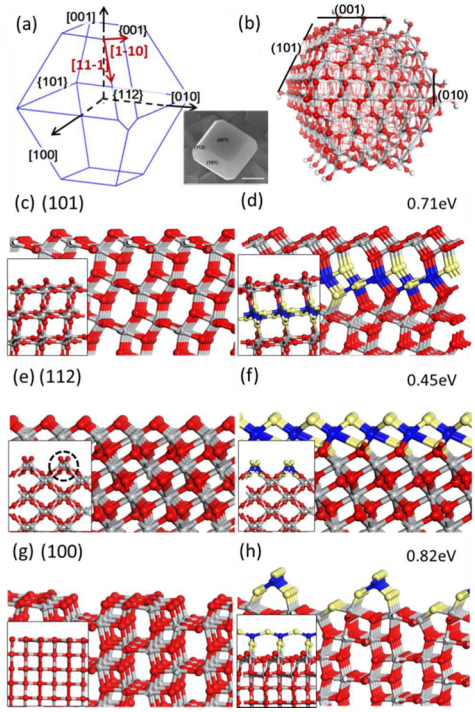

Figure 2. Common anatase surfaces before (left in c–h) and after (right in c–h) the surface reconstruction as identified from SSW PES exploration. (a and b) Typical decahedral morphology of anatase particles (shown in the inset is the SEM picture adapted from ref 48 (Copyright 2014 with permission from Nature Publishing Group) and the atomic model;[49] (c and d) (101) surface; (e and f) (112) surface; (g and h) (100) surface. The insert in (c–h) is another side view of the surfaces. Blue: Ti after reconstruction; gray: Ti before reconstruction; yellow: O after reconstruction; and red: O before reconstruction.

In SSW simulation, each surface slab contains 15 layers with more than 90 atoms (see Supporting Information for the structure), and only one side of the slab (i.e., the top 6 layers) is allowed to reconstruct (relax). For each surface, over 50,000 minima nearby the unreconstructed surface are visited, from which the likely surface restructuring patterns are collected. We found that among the four surfaces studied ((101), (001), (100), and (112)), three surface facets can undergo obvious reconstruction, i.e., (101), (100), and (112). The structures of the surfaces before and after the reconstruction are summarized in Figure 2c–h.

For (101) surface, the major pattern of surface reconstruction is to form a (101)-twin, where the [001] direction of the original phase is rotated by 45° (Figure 1c,d). Our DFT calculations show that a thin-layer (101)-twin surface (Figure 1d) is in fact less stable by 0.71 eV per (2 × 1) surface than the unreconstructed surface, indicating the unreconstructed (101) surface is already rather stable. This is consistent with the experimental observation that the (101) facet (Figure 2a) is the most stable surface under the hydrothermal conditions. The (101)-twin can grow by the oriented attachment of two anatase particles as observed in HRTEM experiment (see, e.g., Penn,[11] Zhang,[42,43] and Li[44]).

For (112) surface, we found several possible surface structure configurations depending on the layer thickness of the reconstructing. The most common pattern is to yield a one-layer TiO_2-II-like surface structure, as shown in Figure 2e,f. The reconstructed surface is 0.45 eV per (1 × 1) less stable than the unreconstructed surface from DFT. In addition to the first-layer reconstructing, we found that the restructuring can proceed progressively into the anatase bulk, leading to the formation of TiO_2-II phase or brookite phase on the surface. This indicates that (112) surface is the surface facet that can initiate the anatase phase transition. The detailed kinetics are present in the next section.

For (100) surface, we found a complex ad-row reconstruction pattern featuring a (1 × 1) TiO_4 row on the surface: each Ti is only four-coordinated compared to the original five-coordinated Ti on the unreconstructed surface. In the TiO_4, the bond length of Ti–O bond increases to 2.19 Å, being 0.24 Å longer than the typical Ti–O distance in the anatase bulk. The reconstruction is energetically unfavorable, being 0.82 eV per (1 × 1) surface less stable after restructuring. Indeed, we did not find any experimental evidence for such reconstructed anatase (100). We noticed that very similar ad-row reconstruction has been observed in the experiment for anatase (001) surface,[45–47] suggesting the potential to form a four-coordinated TiO_4 row on the anatase surface. However, we did not observe any (001) reconstruction in SSW simulation, which could be attributed to the fact that the number of surface atoms is maintained in SSW simulation, while half of the surface atoms need to be removed in the (001) ad-row reconstruction observed in experiment. Nevertheless, such ad-row reconstruction patterns cannot propagate into the anatase bulk, and thus {100} and {001} can be ruled out as the candidates for the nucleation site of anatase-to-rutile phase transition.

3.2. Mechanism of Phase Transition Initiating from Anatase (112). Here, we will focus on anatase (112) surface since its reconstruction can lead to the new phase that propagates into the anatase bulk, while the other surfaces exhibit only the surface layer restructuring. To reveal how new

DOI: 10.1021/jacs.5b07734
J. Am. Chem. Soc. 2015, 137, 11532–11539

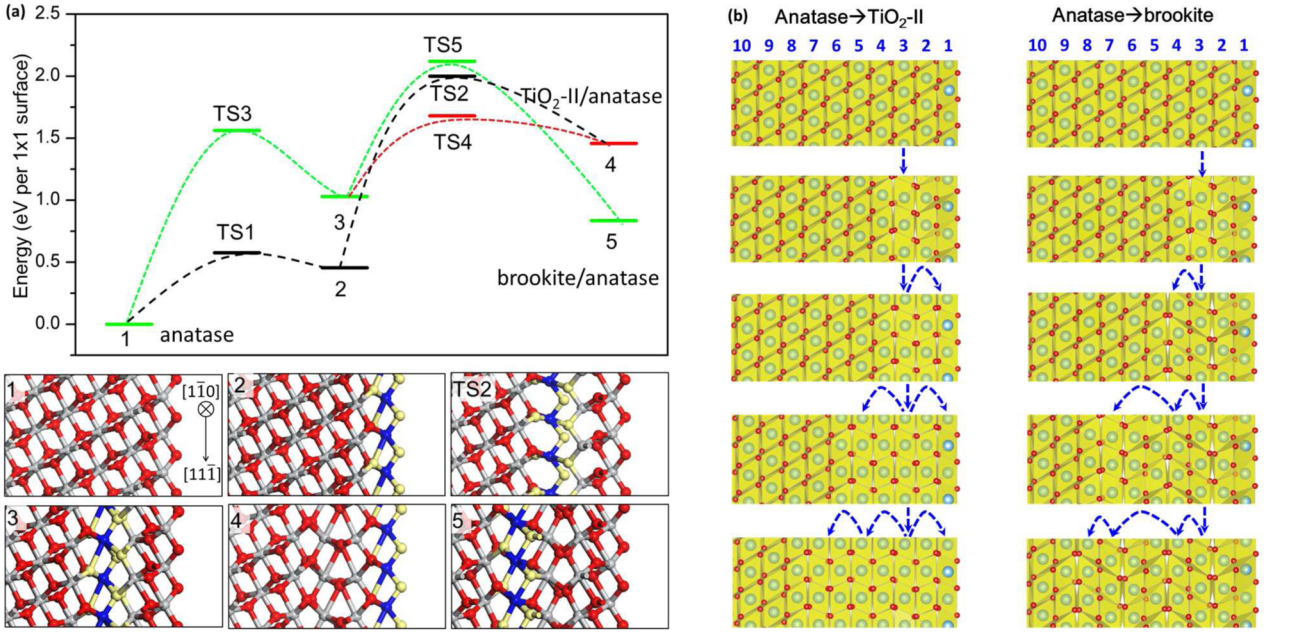

Figure 3. (a) DFT energy profile and key structures for the anatase (112) reconstruction that leads to the formation of TiO_2-II and brookite phases. The color scheme is the same as Figure 2. (b) Scheme for the mechanism of phase transition starting from anatase (112) surface as represented by TiO_6 octahedrons. The arrows indicate the layer position of restructuring during the phase transition. All views are looking down from anatase [1$\bar{1}$0]. The animations of the pathways are also shown in Supporting Information.

phases gradually grow upon anatase (112), the SSW pathway sampling simulation was carried out iteratively by following the likely low-energy pathways. The procedure is described briefly in the following.

We started from the (1 × 1) unreconstructed (112) surface and utilized SSW to explore the possible pathways leading to the change of surface structure. After obtaining the likely IS/FS pairs (>5000 pairs), we then searched for the TS of all these reactions using the DESW method. By sorting the reaction barrier of the pathways, we can identify a few distinct low-energy pathways, which may lead to different product phases. We need to repeat the whole procedure by starting from the product phase of the selected low-energy pathways. This will eventually establish the reaction network of surface reconstruction. Finally, by comparing the effective barrier of the pathways (the energy difference between the highest energy position along the pathway and the initial unreconstructed surface), we can finally determine the lowest energy pathways that determine the phase transformation kinetics. Figure 3a summarizes the DFT energetics of the phase transformation up to the fourth surface layer, where the structures for the important intermediate are also shown.

In total, we identify three low-energy pathways, namely, Paths I, II, and III, which lead to two different surface phases, TiO_2-II and brookite, on the anatase (112) surface. Path I has the lowest barrier for the first-layer surface reconstruction; Path II has the lowest effective barrier to form TiO_2-II phase; and Path III has the lowest effective barrier to form brookite phase.

Specifically, Path I involves the first-layer reconstruction (state **1** to state **2** in Figure 3) and the subsequent second−third layer reconstruction to TiO_2-II (state **2** to state **4**); Both Paths II and III first involve the subsurface two-layer reconstruction (state **1** to state **3** in Figure 3). It then follows the first-layer reconstruction (**3** to **4**) in Path II to yield TiO_2-II, while it is continued by the fourth-layer reconstruction (**3** to **5**) to form brookite in Path III.

Starting from the unreconstructed surface, the **1** to **2** first-layer reconstruction has the lowest barrier, being 0.57 eV per (1 × 1) surface from DFT. Due to the endothermic nature of the reaction, the reverse reaction is kinetically more facile with only 0.2 eV barrier. The reconstruction occurs mainly via a collective movement of the two-coordinated O (O_{2c}) and the five-coordinated Ti (Ti_{5c}) on the surface. In the reaction, the Ti_{5c} and its neighboring O_{2c} shift along the [11$\bar{1}$] direction by ∼1 Å, but the neighboring O_{3c} shifts toward the opposite direction by ∼0.5 Å. To maintain the bonding with the underneath anatase framework, the O_{2c} atoms, along with the translational shift, also rotate around the Ti_{5c} by 37°, crossing the ($\bar{1}$10) plane. This yields a zigzag pattern for O_{2c} movement. Further starting from state **2**, the product of the first-layer reconstruction, the dominant pathway found from SSW pathway sampling, is the reverse reaction back to the unreconstructed surface. There is also a minor reaction channel to form state **4** from state **2**, which however has a higher overall barrier than Path II to form TiO_2-II phase (discussed below). No other low-energy pathway can be identified for the new phase formation into the anatase bulk. Apparently, the first-layer reconstruction can be regarded as a fast-equilibrium reversible reaction for its much lower barrier than other steps.

For the subsurface two-layer reconstruction (**1** to **3**), the reaction occurs by transforming two anatase subsurface layers to the TiO_2-II-like structure (state **3**). The calculated reaction barrier is 1.56 eV per (1 × 1) surface, and the reaction is endothermic by 1.01 eV per (1 × 1) surface (Figure 3). The endothermic nature and the high barrier to form the nucleus are consistent with the slow kinetics of anatase-to-rutile phase transition, which typically occurs above 900 °C in dry conditions (see Figure 1a). The crystallographic orientation relation (OR) for the phase transition can be described as $(112)_A//(100)_{II}$, $[\bar{1}10]_A//[010]_{II}$. In the transformation, the third-layer Ti_{6c} and its neighboring O_{3c} shift along [11$\bar{1}$] direction by ∼1 Å. To maintain the bonding with the anatase

DOI: 10.1021/jacs.5b07734
J. Am. Chem. Soc. 2015, 137, 11532−11539

framework, the surface (first-second layer) Ti and O also move along the $[11\bar{1}]$ direction by ~2.7 Å, about half of the surface lattice length, along with the translational move of the third-layer atoms.

Starting from the product structure (state **3**) of the subsurface two-layer reconstruction, interestingly, there are two different pathways, one leading to the formation of the less stable TiO_2-II phase with lower reaction barrier (state **3** to state **4**) and another leading to the more stable brookite phase (state **3** to state **5**) but with higher reaction barrier. It should be mentioned that the brookite phase is not observed as the intermediate in the homogeneous-phase transition pathway from anatase to rutile in our previous work.[31]

In fact, the reaction from state **3** to state **4** is the same as the first-layer reconstruction as described above from the unreconstructed anatase (112) surface. This is apparently because the reaction from state **3** to state **4** involves only the first-layer reconstruction without changing the subsurface surface structure. In state **3**, the subsurface layers, i.e., second−third layers, are TiO_2-II like, whereas in state **4**, all the top three layers become TiO_2-II like. The reaction barrier is 0.65 eV with respect to state **3**, and the overall barrier to form three-layer TiO_2-II is 1.68 eV with respect to the unreconstructed (112) surface.

By contrast, the reaction from state **3** to state **5** initiates by the fourth-layer atomic displacement, which follows the reaction pattern similar to that from state **1** to state **3.** The fourth-layer Ti_{6c} and its neighboring O_{3c} atoms shift along the $[11\bar{1}]$ direction by ~1.3 Å, and the surface (first−third layer) Ti and O move along $[11\bar{1}]$ direction by ~2.7 Å, about half of the length of the surface lattice. The crystallographic OR for the transformation is $(112)_A//(100)_B$, $[\bar{1}10]_A//[010]_B$. The reaction barrier is 1.09 eV with respect to state **3**, and the overall barrier to form four-layer brookite is 2.12 eV with respect to the unreconstructed (112) surface.

The above results indicate that two different new phases, TiO_2-II and brookite, can grow upon anatase (112) via collective shear movement of surface atoms. TiO_2-II is the kinetically preferred product. The overall atom displacement patterns can be summarized in the Figure 3b, which highlights that TiO_6 octahedrons along $[11\bar{1}]$ reverse their axial direction in the phase transition. According to the lowest energy pathways, we can conclude that the formation of TiO_2-II phase is induced by the odd layer (i.e., first, third, fifth, seventh, etc.) atom movement of anatase (112) surface. On the other hand, the formation of brookite phase is caused by both the odd and the even layers (i.e., third, fourth, seventh, eighth, etc.) atom movement. The atom displacement is dominated by the shearing movement along $[11\bar{1}]$ direction that propagates gradually deep into the bulk, exhibiting a typical anisotropic characteristics of solid phase transition.

The differences in the pathway to TiO_2-II and brookite can be attributed to the intrinsic symmetry difference of anatase, TiO_2-II, and brookite. Because brookite can be regarded as a half−half phase in between TiO_2-II and anatase from the stacking arrangement of TiO_6 octahedrons, the phase transformation from anatase to brookite is required to first create TiO_2-II like layers on the anatase surface, which involves the odd layer reconstruction. The subsequent reconstruction of the neighboring even layer will finally create the brookite phase.

3.3. Anisotropic Behavior in Phase Transformation. To provide deeper insights into the anisotropic kinetics of the phase transition, we further investigated the kinetics of (112) surface-phase transition using doubled ((1 × 2) and (2 × 1)) supercells along two directions, i.e., $[11\bar{1}]$ (**SC-1**) and $[1\bar{1}0]$ (**SC-2**). As the formation of TiO_2-II is kinetically preferred, we focus on the reaction pathway to form the subsurface TiO_2-II, i.e., corresponding to the reaction from state **1** to **3** in (1 × 1) cell (Figure 3).

For the two supercells, **SC-1** and **SC-2**, we have investigated the phase transition using two different sets of lattice parameters, namely in the bulk anatase lattice and in a compressed lattice with the TiO_2-II lattice parameter. Compared to anatase phase, TiO_2-II, being a high-pressure phase, has 11.6% contraction at $[11\bar{1}]$ and 2.3% expansion at $[1\bar{1}0]$ directions, respectively. The presence of compressive strain is likely during phase transition because of the relaxation of the nascent TiO_2-II phase and also the interaction between small nanoparticles. By using a different set of lattice parameters, we are able to examine the possible strain effect on the phase transition kinetics.

For the phase transition with the anatase bulk lattice parameter, we found that the pathway to form TiO_2-II phase has the similar reaction barrier for **SC-1** and **SC-2**, showing no appreciable anisotropic behavior (as shown in Supporting Information Figure S1). For the compressed lattice, the phase transition energy profile for **SC-1** is shown in the red curve of Figure 4, which is compared with that for **SC-2** shown in the black curve. We found that (i) the overall barrier is much reduced compared to that in the bulk anatase lattice; (ii) the pathway to form TiO_2-II phase in **SC-1** has a much higher barrier than that in **SC-2**. The (i) is apparently caused by the

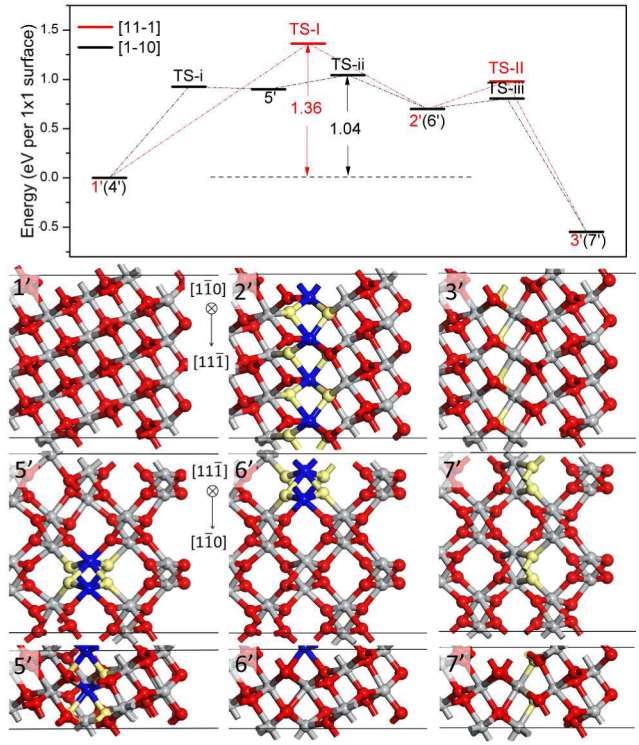

Figure 4. DFT energy profile for the phase transition from anatase to TiO_2-II in doubled supercells of anatase (112) under a compressive strain (in TiO_2-II bulk lattice). Two side views are shown for **5′**, **6′**, and **7′** states. Red curve: **SC-1** with doubled supercell at the $[11\bar{1}]$ direction; black curve: **SC-2** with doubled supercell at the $[1\bar{1}0]$ direction. The color scheme of atoms is the same as Figure 2.

DOI: 10.1021/jacs.5b07734
J. Am. Chem. Soc. 2015, 137, 11532−11539

thermodynamics to favor the formation of TiO_2-II in the compressed lattice, while the (ii) indicates that the reaction barrier increases with the increase of the length of the supercell at the $[11\bar{1}]$ direction, the shear direction of phase transition. These results are elaborated in the following.

The reaction pathways for **SC-1** and **SC-2** are quite similar to the (1 × 1) pathway from state **1** to state **3** shown in Figure 3, except that more intermediate states emerge after the cell doubling. For example, the **SC-1** pathway differs from the (1 × 1) pathway by the new intermediate state **2′** (see Figure 4), where the Ti atoms at the third layer shifts ∼0.5 Å at the $[11\bar{1}]$ direction and the O shifts only ∼1 Å. On the other hand, in the **SC-2** pathway, the phase transition can be separated into sequential transition steps, each with localized structure change in one ridge of (112) (also see Figure 2e insert, black circle). For example, only half of the (112) ridge at the third layer undergoes the reconstruction at the intermediate state **5′** (in Figure 4), and it is not until state **6′** that the reconstruction is completed for the third layer.

By comparing the reaction barrier of **SC-1** and **SC-2**, we can conclude that the phase propagation along the $[11\bar{1}]$ direction is slower than it was along the $[1\bar{1}0]$ direction. It is thus expected that anatase nanoparticles with long $[11\bar{1}]$ ridges, i.e., sharp particle (see Figures 1a and 2a), could be more stable and kinetically slower in the phase transition. This anisotropic behavior is consistent with the experimental finding.[4] We will discuss this in more detail in Section 4.2.

4. DISCUSSION

4.1. Nature of Rutile Nuclei. Great efforts have been devoted to determine the structure of rutile nuclei that emerge at the initial stage of the anatase-to-rutile phase transition. Banfield's group[25] has managed to identify two different new phases, both called "rutile nuclei", which were found to attach with the (112) planes of anatase particles under hydrothermal conditions (250 °C). The first type of rutile nuclei is a thin slab inside anatase (112) twin, as reported in ref 25 (also see Figure 5a). Its structure is distinct from a slab of brookite, as verified by comparisons to both image simulations and HRTEM images of brookite in relevant orientations. The atomic structure cannot be clearly determined from XRD (this is because the anatase + TiO_2-II and anatase + brookite mixed phases have very similar XRD pattern, see Figure S2 in Supporting Information). The second type of rutile nuclei was characterized as a brookite phase slab inside anatase[24] (also see Figure 5b). The slab is much thicker than the first type of nuclei. Interestingly, the rutile nuclei seem not rutile in both cases, implying the presence of intermediate phases in anatase-to-rutile phase transition. But, it remains unclear which structure is truly responsible for the phase transition.

Our SSW pathway sampling results can be utilized to assign the atomic structures of the rutile nuclei. The two types of rutile nuclei observed in experiment should correspond to TiO_2-II phase and brookite phase according to Figure 3. We further confirm this by comparing theoretically simulated HRTEM pictures with the experimental pictures of Banfield's group. According to the determined OR, we have constructed the atomic model for antase/TiO_2-II/anatase and anatase/brookite/anatase interfaces and simulate the HRTEM picture of these interfaces using the JEMS software.[50] The simulated pictures are shown in Figure 5c,d. As shown, the simulated images showed lattice fringes closely resembling the observed ones, indicating that the theoretical models can reproduce well

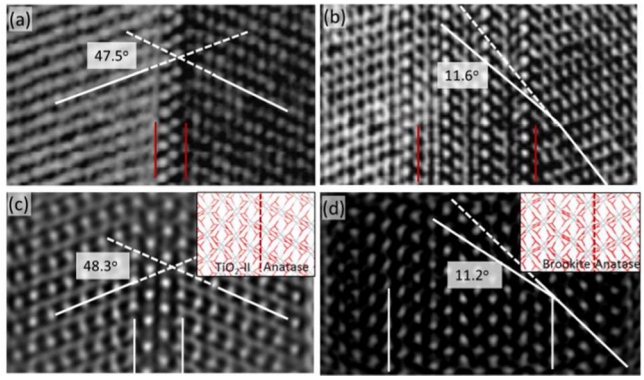

Figure 5. Comparison of experimental HRTEM (a and b) and simulated HRTEM (c and d) images for two likely structures of rutile nuclei in the twinned anatase particle. All views are looking down from anatase [131]. (a) anatase/TiO2-II,[25] (Copyright 1999, with permission from Mineralogical Society of America). (b) Anatase/brookite.[24] (Copyright 1998, with permission from Mineralogical Society of America). (c) Simulated HRTEM of anatase/TiO_2-II junction with OR $(112)_A//(100)_{II}$, $[1\bar{1}0]_A//[010]_{II}$. (d) Simulated HRTEM of anatase/brookite junction with OR $(112)_A//(100)_B$, $[1\bar{1}0]_A//[010]_B$. The inserts in (c and d) are the atomic models of the junctions utilized for HRTEM simulation.

with the experimental structure. Specifically, the dihedral angle between {101} planes of anatase twins in antase/TiO_2-II/anatase is 48.3° as predicted from theory and 47.5° in experiment. The dihedral angle between anatase (101) and brookite (211) in anatase/brookite/anatase is 11.2° from theory and is 11.6° in experiment.

Our results suggest that both TiO_2-II and brookite phases can be present at the initial stage of anatase-to-rutile phase transition. From thermodynamics, TiO_2-II bulk as a high-pressure phase is less stable than brookite bulk. However, since the nascent rutile nuclei coexist with anatase phase as thin slabs, it is still essential to consider the interface energy when addressing the stability of the nuclei. To this end, we have computed the interface energy of anatase/II and anatase/brookite junction by constructing the biphase superlattice based on the theoretical approach proposed previously[51] (the interface energy is given by $\gamma = (E_{tot} - E_a - E_b)/2S$, where S is the interface area, $E_{a/b}$ are the energies of parent phases, and E_{tot} is the energies of the mixed phase). Our DFT calculated interface energy is 0.19 and 0.07 J/m^2 for a 4anatase/4II interface (four-layer anatase and four-layer TiO_2-II in a superlattice) and 4anatase/4brookite interface (four-layer anatase and four-layer brookite in a superlattice), respectively. The lower interface energy of anatase/brookite junction is consistent with the energy profile in Figure 3, where the brookite thin slab on anatase is more stable than the TiO_2-II slab on anatase.

Although thermodynamically less stable, TiO_2-II on anatase (112) is the kinetically preferred product of phase transition for its lower barrier of surface restructuring. Our previous work on the homogeneous-phase transition pathway of TiO_2 crystals show that TiO_2-II is the intermediate connecting anatase with rutile.[31] The formation of TiO_2-II is the key step toward the formation of rutile, and the TiO_2-II thin slab in anatase is thus the true rutile nucleus. The brookite phase, however, is the byproduct from the bifurcate channels. From the potential energy diagram in Figure 3, the nascent brookite can transform easily back to anatase and then form TiO_2-II. Consequently,

DOI: 10.1021/jacs.5b07734
J. Am. Chem. Soc. 2015, 137, 11532−11539

even the brookite is formed from anatase, it will eventually transform to rutile via TiO_2-II phase under the phase transition conditions.

4.2. The Anisotropic Kinetics of Anatase-to-Rutile Phase Transition. Finally, we are at the position to discuss the anisotropic kinetics of anatase-to-rutile transition in the context of experimental findings. As shown in Figure 1a, Zhao et al.[4] found that rutile formation temperature drops by ~100 °C when the (001) concentration of anatase nanoparticles increase from 32% to 63%. Consistent with this finding, the particle size effect on the phase transition barrier was also derived from experiment by Zhang et al.,[11] who showed that when the particle size decreases from 22 to 8 nm, the phase transition barrier decreases by ~0.2 eV (20 kJ/mol) from 220 to 200 kJ/mol (see Figure S3 in Supporting Information). Our theoretical results show that the presence of strain and the length of $[11\bar{1}]$ are critical to the phase transition kinetics. The compressive strain and short $[11\bar{1}]$ ridge length will help to reduce the phase transition barrier.

We can summarize the anisotropic kinetics of anatase-to-rutile phase transition using Figure 6, where the nanoparticle

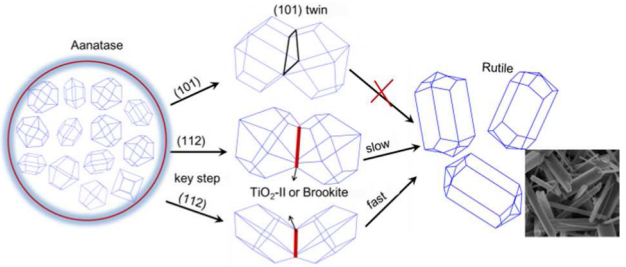

Figure 6. A macroscopic scheme illustrating the structure evolution for anatase-to-rutile phase transition, the kinetics of which is sensitive to crystallographic facets and the anatase particle size/morphology. Also shown is a typical SEM picture of rutile particle.[29]

size/morphology and the contacting surface facets matter in the phase transition kinetics. Our results confirm that anatase (112) is the key facet responsible for the anatase-to-rutile phase transition. The origin of the facet dependence of the phase transition can be attributed to the allowed atomic displacement pattern in the phase transition, where (112) surface has the lowest transition barrier to reconstruct to new phases. The growth (ripening) of small anatase particles by joining their (112) facets will change the local strain at the contacting area. The compressive strain, if developed at the interface region, will help to initiate the phase transition to yield thin rutile nucleus, TiO_2-II slabs.

Because (112) facet is the ridges connecting neighboring {101} in anatase nanoparticles, the phase transition kinetics is sensitive to the nanoparticle size, i.e., the length of the ridge. Our DFT pathways in Figure 4 showed that the long ridge, i.e., long distance at the $[11\bar{1}]$ direction, is kinetically more difficult in phase transition compared to the short ridge. On the other hand, the width of the ridge, as measured by the $[1\bar{1}0]$ length, has little effect on the phase transition kinetics. Overall, the small nanoparticles with short (112) ridges (a flat shaped particle dominated by (001) facets) are kinetically faster in the phase transition, where the reduction in the reaction barrier is up to 0.3 eV (with the compressed lattice). This value agrees reasonably with the measured data in the experiment (~20 kJ/mol)[11] and a reduction of phase transition temperature by ~100 K.[4]

5. CONCLUSIONS

This work resolves the structure of rutile nuclei that initiate the anatase-to-rutile phase transition. The recently developed SSW PES exploration method is utilized to sample the surface reconstruction pathways. We show that the rutile nucleus is nascent TiO_2-II thin slab other than anatase and rutile. Among common anatase surfaces, anatase (112) is the only surface that can reconstruct to the new phases, TiO_2-II phase and brookite phase. TiO_2-II phase is the kinetically preferred product of the phase transition, while brookite phase is thermodynamically more stable. In combination with our previous work of homogeneous phase transition mechanism, the thin TiO_2-II slab is determined as the true rutile nucleus that is responsible for the anatase-to-rutile phase transition. The brookite phase is the byproduct in the anatase-to-rutile phase transition. The current results rationalize the particle size and morphology dependence of phase transition kinetics and could facilitate the rational design of solid materials via controlled solid phase transition kinetics (e.g., by opening/blocking particular surface sites, (112) surface in this work). The key results are further outlined as follows.

(i) The crystallographic OR of the initial phase transition is $(112)_A//(100)_{II}$, $[1\bar{1}0]_A//[010]_{II}$ for anatase/TiO_2-II and $(112)_A//(100)_B$, $[1\bar{1}0]_A//[010]_B$ for anatase/brookite.

(ii) The phase transition is hindered by a high reaction barrier at the initial stage to form the nucleus, which is calculated to be 1.68 eV per (1×1) anatase (112) surface for anatase to TiO_2-II and 2.12 eV per (1×1) for anatase to brookite.

(iii) The phase transition is highly sensitive to the local strain. An ~11.6% compressive strain at $[11\bar{1}]$ can reduce significantly the reaction barrier of phase transition to 1.04 eV per (1×1).

(iv) In the presence of compressive strain, the phase transition becomes highly anisotropic with much higher energy barrier for the phase propagation along $[11\bar{1}]$ direction compared to that along the $[1\bar{1}0]$.

■ ASSOCIATED CONTENT

Supporting Information

The Supporting Information is available free of charge on the ACS Publications website at DOI: 10.1021/jacs.5b07734.

Energy profile of doubled supercells of anatase (112) in bulk anatase lattice; experimental XRD pattern and simulated XRD pattern; the relation of particle size and the phase transition barrier from experiment; and XYZ coordinates of the pathways reported (PDF)

Animation of pathways in Figure 3 (PPTX)

■ AUTHOR INFORMATION

Corresponding Author

*zpliu@fudan.edu.cn

Notes

The authors declare no competing financial interest.

DOI: 10.1021/jacs.5b07734
J. Am. Chem. Soc. 2015, 137, 11532−11539

■ ACKNOWLEDGMENTS

This work is supported by National Science Foundation of China (21173051, 21361130019, 21533001), 973 program (2011CB808500, 2013CB834603), Science and Technology Commission of Shanghai Municipality (08DZ2270500), and Program for Professor of Special Appointment (Eastern Scholar) at Shanghai Institute of Higher Learning.

■ REFERENCES

(1) Li, Y. F.; Liu, Z. P.; Liu, L. L.; Gao, W. G. *J. Am. Chem. Soc.* **2010**, *132*, 13008−13015.
(2) Tay, Q. L.; Liu, X.; Tang, Y.; Jiang, Z.; Sum, T. C.; Chen, Z. *J. Phys. Chem. C* **2013**, *117*, 14973−14982.
(3) Zhang, J.; Xu, Q.; Feng, Z.; Li, M.; Li, C. *Angew. Chem., Int. Ed.* **2008**, *47*, 1766−9.
(4) Zhao, Y. B.; Zhang, Y. F.; Liu, H. W.; Ji, H. W.; Ma, W. H.; Chen, C. C.; Zhu, H. Y.; Zhao, J. C. *Chem. Mater.* **2014**, *26*, 1014−1018.
(5) Gouma, P. I.; Mills, M. l. J. *J. Am. Ceram. Soc.* **2001**, *84*, 619−622.
(6) Linsebigler, A. L.; Lu, G. Q.; Yates, J. T. *Chem. Rev.* **1995**, *95*, 735−758.
(7) Koparde, V. N.; Cummings, P. T. *ACS Nano* **2008**, *2*, 1620−1624.
(8) Zhang, H.; Banfield, J. F. *Chem. Rev.* **2014**, *114*, 9613−9644.
(9) Zhang, H.; Banfield, J. F. *J. Phys. Chem. B* **2000**, *104*, 3481−3487.
(10) Gilbert, B.; Zhang, H. Z.; Huang, F.; Finnegan, M. P.; Waychunas, G. A.; Banfield, J. F. *Geochem. Trans.* **2003**, *4*, 20−27.
(11) Zhang, H. Z.; Banfield, J. F. *Chem. Mater.* **2005**, *17*, 3421−3425.
(12) Zhang, H. Z.; Banfield, J. F. *J. Mater. Res.* **2000**, *15*, 437−448.
(13) Gribb, A. A.; Banfield, J. F. *Am. Mineral.* **1997**, *82*, 717−728.
(14) Zhang, H. Z.; Banfield, J. F. *Am. Mineral.* **1999**, *84*, 528−535.
(15) Zhang, J.; Li, M. J.; Feng, Z. C.; Chen, J.; Li, C. *J. Phys. Chem. B* **2006**, *110*, 927−935.
(16) Zhang, J.; Xu, Q.; Li, M.; Feng, Z.; Li, C. *J. Phys. Chem. C* **2009**, *113*, 1698−1704.
(17) Penn, R. L.; Banfield, J. F. *Science* **1998**, *281*, 969−971.
(18) Chaudhuri, J.; Ram, M.; Sarkar, B. *J. Mater. Sci.* **1994**, *29*, 3484−3488.
(19) Napolitano, E.; Mulas, G.; Enzo, S.; Delogu, F. *Acta Mater.* **2010**, *58*, 3798−3804.
(20) Begin-Colin, S.; Girot, T.; Mocellin, A.; Le Caër, G. *Nanostruct. Mater.* **1999**, *12*, 195−198.
(21) BeHgin-Colin, S.; Girot, T.; Le CaeKr, G.; Mocellin, A. *J. Solid State Chem.* **2000**, *149*, 48.
(22) Dutta, H.; Sahu, P.; Pradhan, S.; De, M. *Mater. Chem. Phys.* **2003**, *77*, 153−164.
(23) Ricci, P. C.; Carbonaro, C. M.; Stagi, L.; Salis, M.; Casu, A.; Enzo, S.; Delogu, F. *J. Phys. Chem. C* **2013**, *117*, 7850−7857.
(24) Penn, R. L.; Banfield, J. F. *Am. Mineral.* **1998**, *83*, 1077−1082.
(25) Penn, R. L.; Banfield, J. F. *Am. Mineral.* **1999**, *84*, 871−876.
(26) Zhou, Y.; Fichthorn, K. A. *J. Phys. Chem. C* **2012**, *116*, 8314−8321.
(27) Xu, Q.; Zhang, J.; Feng, Z.; Ma, Y.; Wang, X.; Li, C. *Chem. - Asian J.* **2010**, *5*, 2158−2161.
(28) Dubrovinskaia, N. A.; Dubrovinsky, L.; Ahuja, R.; Prokopenko, V.; Dmitriev, V.; Weber, H. P.; Osorio-Guillen, J.; Johansson, B. *Phys. Rev. Lett.* **2001**, *87*, 275501−275504.
(29) Zhu, S. C.; Xie, S. H.; Liu, Z. P. *J. Phys. Chem. Lett.* **2014**, *5*, 3162−3168.
(30) Shang, C.; Zhang, X. J.; Liu, Z. P. *Phys. Chem. Chem. Phys.* **2014**, *16*, 17845−56.
(31) Shang, C.; Zhao, W. N.; Liu, Z. P. *J. Phys.: Condens. Matter* **2015**, *27*, 134203.
(32) Shang, C.; Liu, Z. P. *J. Chem. Theory Comput.* **2013**, *9*, 1838−1845.
(33) Zhang, X. J.; Shang, C.; Liu, Z. P. *J. Chem. Theory Comput.* **2013**, *9*, 5745.
(34) Zhang, X. J.; Shang, C.; Liu, Z. P. *J. Chem. Theory Comput.* **2013**, *9*, 3252−3260.
(35) Guan, S. H.; Zhang, X. J.; Liu, Z. P. *J. Am. Chem. Soc.* **2015**, *137*, 8010−8013.
(36) Shang, C.; Liu, Z. P. *J. Chem. Theory Comput.* **2010**, *6*, 1136−1144.
(37) Matsui, M.; Akaogi, M. *Mol. Simul.* **1991**, *6*, 239−244.
(38) Junquera, J.; Paz, O.; Sanchez-Portal, D.; Artacho, E. *Phys. Rev. B: Condens. Matter Mater. Phys.* **2001**, *64*, 235111−235119.
(39) Anglada, E.; Soler, J. M.; Junquera, J.; Artacho, E. *Phys. Rev. B: Condens. Matter Mater. Phys.* **2002**, *66*, 205101−205104.
(40) Perdew, J. P.; Burke, K.; Ernzerhof, M. *Phys. Rev. Lett.* **1996**, *77*, 3865−3868.
(41) Monkhorst, H. J.; Pack, J. D. *Phys. Rev. B* **1976**, *13*, 5188−5192.
(42) Zhang, H.; Banfield, J. F. *J. Phys. Chem. Lett.* **2012**, *3*, 2882−2886.
(43) Zhang, H.; De Yoreo, J. J.; Banfield, J. F. *ACS Nano* **2014**, *8*, 6526−6530.
(44) Li, D. S.; Soberanis, F.; Fu, J.; Hou, W. T.; Wu, J. Z.; Kisailus, D. *Cryst. Growth Des.* **2013**, *13*, 422−428.
(45) Xia, Y.; Zhu, K.; Kaspar, T. C.; Du, Y.; Birmingham, B.; Park, K. T.; Zhang, Z. *J. Phys. Chem. Lett.* **2013**, *4*, 2958−2963.
(46) Herman, G. S.; Sievers, M. R.; Gao, Y. *Phys. Rev. Lett.* **2000**, *84*, 3354−3357.
(47) Lazzeri, M.; Selloni, A. *Phys. Rev. Lett.* **2001**, *87*, 266105.
(48) Yang, S.; Yang, B. X.; Wu, L.; Li, Y. H.; Liu, P.; Zhao, H.; Yu, Y. Y.; Gong, X. Q.; Yang, H. G. *Nat. Commun.* **2014**, *5*, 5355.
(49) Li, Y. F.; Liu, Z. P. *J. Am. Chem. Soc.* **2011**, *133*, 15743−15752.
(50) Dutto, F.; Heiss, M.; Lovera, A.; Lopez-Sanchez, O.; Fontcuberta i Morral, A.; Radenovic, A. *Nano Lett.* **2013**, *13*, 6048−6054.
(51) Zhao, W. N.; Zhu, S. C.; Li, Y. F.; Liu, Z. P. *Chem. Sci.* **2015**, *6*, 3483−3494.

DOI: 10.1021/jacs.5b07734
J. Am. Chem. Soc. 2015, 137, 11532−11539